PNAS RESEARCH ARTICLE | DEVELOPMENTAL BIOLOGY

Samd7 represses short-wavelength cone genes to preserve long-wavelength cone and rod photoreceptor identity

Leo I. Volkov[a], Yohey Ogawa[a], Ramiz Somjee[a], Hannah E. Vedder[a], Hannah E. Powell[a], Deepak Poria[b], Sam Meiselman[a], Vladimir J. Kefalov[b], and Joseph C. Corbo[a,1]

Edited by Jeremy Nathans, Johns Hopkins University School of Medicine, Baltimore, MD; received January 30, 2024; accepted September 16, 2024

The role of transcription factors in photoreceptor gene regulation is fairly well understood, but knowledge of the cell-type-specific function of transcriptional cofactors remains incomplete. Here, we show that the transcriptional corepressor *samd7* promotes rod differentiation and represses short-wavelength cone genes in long-wavelength cones in zebrafish. In *samd7*$^{-/-}$ retinas, red cones are transformed into hybrid red/ultraviolet (UV) cones, green cones are absent, the number of blue cones is approximately doubled, and the number of rods is greatly reduced. We also find that mouse *Samd7* represses S-opsin expression in dorsal M-cones—analogous to its role in repressing UV cone genes in zebrafish red cones. Thus, *samd7* plays a key role in ensuring appropriate patterns of gene expression in rods and cone subtypes of both zebrafish and mice.

retina | photoreceptor | development

Significance

Color vision depends on the expression of spectrally distinct opsins across multiple photoreceptor subtypes. Here, we show that the transcriptional corepressor *samd7* acts in both zebrafish and mice to preserve mutually exclusive patterns of opsin expression. In the absence of *samd7*, both species show defects in rod differentiation and aberrant expression of short-wavelength-sensitive cone opsin in long-wavelength-sensitive cones. Zebrafish additionally show loss of green cones and a doubling of the number of blue cones. Together, these studies reveal rod- and cone-subtype-specific functions of *samd7* in zebrafish and mouse retina.

Color vision depends on the differential activation of two or more cone types tuned to different wavelengths of light (1). Differential spectral tuning among cone types is therefore a critical feature of vertebrate retinal development and function. The retina of the common vertebrate ancestor is believed to have possessed one rod type, defined by the expression of rhodopsin (RH1), and four cone types expressing UV opsin (SWS1), blue opsin (SWS2), green opsin (RH2), and red opsin (LWS) (2, 3). Zebrafish (*Danio rerio*) retain a photoreceptor repertoire similar to that of the ancestral vertebrate, with each photoreceptor type expressing distinct opsins and phototransduction components (4–7). Studies in fish have identified multiple transcription factors (TFs) that regulate the specification and diversification of rods and cone types, most notably *nrl, mafba, nr2e3, foxq2, tbx2a, tbx2b, thrb, gdf6a, six6a, six6b,* and *six7* (4, 8–20). Studies in mice have also defined a range of TFs controlling photoreceptor gene expression and subtype specification (e.g., *Otx2, Crx, Rora, Rorb, Nrl, Nr2e3, Casz1, Esrrb, Thrb, Rxrg, NeuroD1, Nr2f1/2 (CoupTFI/II), Pias3, Sall3, Bmal1,* and *Clock*) (21–35). Mutations in vertebrate photoreceptor TFs typically cause one of three phenotypes: 1) gene expression dysregulation, often resulting in cell death; 2) partial cell fate transformation, resulting in formation of a "hybrid" cell type which coexpresses genes of two photoreceptor types; or 3) complete transfating of one photoreceptor subtype into another cell type. For example, mutations in mouse *Nr2e3* transform rods into hybrid cells that coexpress rod and a subset of S-cone genes, while mutations in *Nrl* cause complete conversion of rods into S-cones (23–25). Suppression of alternative photoreceptor cell fates (or gene expression programs) is a common function of cell-type-enriched TFs and may have been a key driver of photoreceptor subtype diversification in evolution (12–14, 24, 25).

In the zebrafish retina, suppression of alternative photoreceptor gene expression programs is necessary to maintain the separate identities of five distinct photoreceptor types (6). In contrast to fish, placental mammals possess a reduced number of photoreceptor types due to evolutionary loss of ancestral blue (SWS2) and green (RH2) cones (7). Most present-day placental mammals therefore possess only three photoreceptor types: rods, UV (SWS1) cones, and red (LWS) cones (7). While the vast majority of mammalian species show mutually exclusive expression of UV and red opsin in the two cone types, the situation in mouse is more complex. Mouse "primordial S-cones" (which exclusively express SWS1 opsin) are present throughout the retina but are concentrated in ventral regions (36, 37). Mouse "M-cones," in contrast, exclusively express LWS opsin ("M-opsin") in the dorsal third of the retina but show coexpression of LWS ("M-opsin") and SWS1 opsin ("S-opsin") in ventral regions (36). Previous studies showed that S-opsin expression is up-regulated in the dorsal M-cones of multiple mouse mutants (28–30, 34, 35), demonstrating that the pattern of cone opsin coexpression is under tight genetic control.

Author affiliations: [a]Department of Pathology and Immunology, Washington University School of Medicine, St. Louis, MO 63110; and [b]Department of Ophthalmology, University of California Irvine, Irvine, CA 92697

Author contributions: L.I.V., Y.O., R.S., D.P., and J.C.C. designed research; L.I.V., Y.O., R.S., H.E.V., H.E.P., D.P., and S.M. performed research; L.I.V., Y.O., and R.S. contributed new reagents/analytic tools; L.I.V., Y.O., R.S., D.P., S.M., and V.J.K. analyzed data; and L.I.V. and J.C.C. wrote the paper.

The authors declare no competing interest.

This article is a PNAS Direct Submission.

[1]To whom correspondence may be addressed. Email: jcorbo@wustl.edu.

This article contains supporting information online at https://www.pnas.org/lookup/suppl/doi:10.1073/pnas.2402121121/-/DCSupplemental.

Published November 12, 2024.

A recent study in mice suggested that *Samd7* might play a key role in these processes. In that paper, the authors showed that mutations in *Samd7* cause upregulation of a subset of cone genes in rods, including S-opsin (38). Samd7 lacks a DNA-binding domain and is thought to act as a transcriptional corepressor by binding the rod-specific TF Nr2e3 and recruiting the polycomb repressive complex 1 (PRC1) to *cis*-regulatory regions of S-cone genes via its sterile alpha motif (SAM) domain (38). Whether *Samd7* plays a comparable role in maintaining cell identity in cones is currently unknown.

To better understand the role of Samd7 in regulating cone photoreceptor cell fate specification and diversification, we created *samd7*$^{-/-}$ zebrafish and evaluated effects on photoreceptor subtype composition and gene expression. We found that *samd7* plays a critical role in the specification of red cones, green cones, and rods by regulating distinct and overlapping patterns of gene expression in these cell types. In the *samd7*$^{-/-}$ retina, red cones are transformed into hybrid red/UV cones, green cones are absent, blue cones are approximately doubled, and most rods fail to differentiate. We also generated *Samd7*$^{-/-}$ mice and analyzed patterns of cone opsin expression in the retina. We found that dorsal M-opsin^{+} cones are transformed into hybrid M/S-cones, resembling the transformation of red to red/UV cones we observe in *samd7*$^{-/-}$ zebrafish. Overall, *Samd7* acts to maintain rod photoreceptor identity and suppress short-wavelength-sensitive cone gene expression in long-wavelength-sensitive cones, thereby preserving normal photoreceptor function.

Results

***Samd7* Is Expressed in Immature Photoreceptors and Mature Red Cones, Green Cones, and Rods.** Previous studies showed *samd7* to be enriched in red cones, green cones, and rods in adult zebrafish retina (4, 5). To determine the expression pattern of *samd7* in larval retina, we used fluorescence-activated cell sorting (FACS) to isolate GFP-expressing cells from the retinas of 4-days-post-fertilization (dpf) *crx:GFP* transgenic zebrafish, which express GFP in developing (immature) and mature photoreceptors and bipolar cells. We then subjected these cells to single-cell RNA sequencing (scRNA-seq). Next, we identified a cluster of immature photoreceptors based on expression of *prdm1a/b,* a marker of early differentiating photoreceptors, and classified photoreceptor subtypes based on cone opsin (*opn1sw1, opn1sw2, opn1mw1,* and *opn1lw2*) and rod opsin (*rho*) expression (*SI Appendix*, Fig. S1) (39, 40). We found that *samd7* is expressed in immature photoreceptors and mature rods, green cones, and red cones but not in UV or blue cones (Fig. 1 *A* and *B*).

To confirm this pattern of *samd7* expression, we performed fluorescent in situ hybridization at 3-dpf, a time point at which

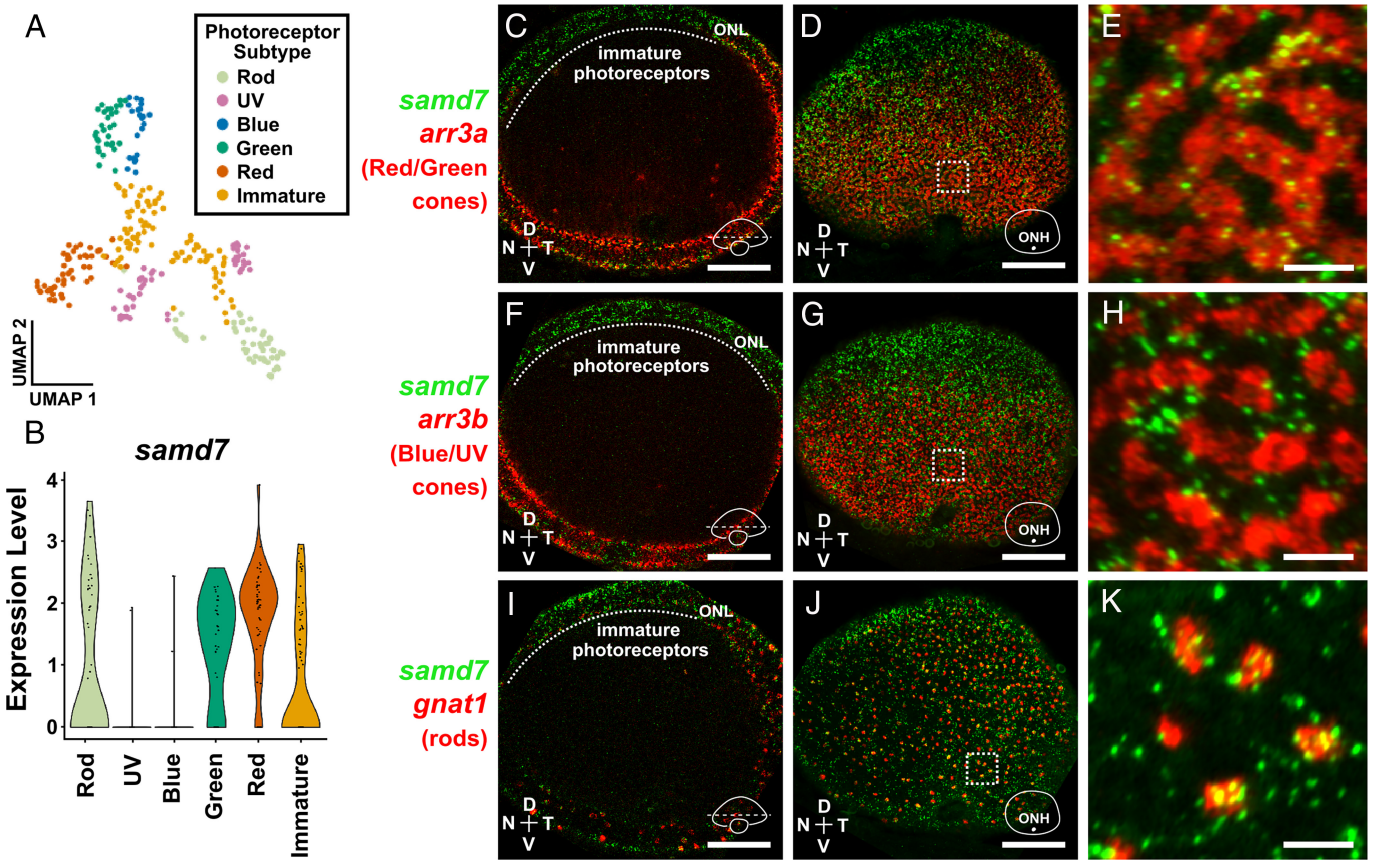

Fig. 1. *Samd7* is expressed in immature photoreceptors, red cones, green cones, and rods in the larval zebrafish retina. (*A*) UMAP (Uniform Manifold Approximation and Projection) of scRNA-seq data from 4-dpf *crx:GFP*$^{+}$ photoreceptors. (*B*) scRNA-seq results show that *samd7* is restricted to immature photoreceptors, red cones, green cones, and rods. See *SI Appendix*, Fig. S1 for detailed expression patterns. (*C*–*K*) Analysis of *samd7* expression in the 3-dpf larval eye by fluorescent in situ hybridization. (*C*) Optical cross-section of the peripheral larval retina stained with probes against *samd7* (green) and red/green-cone-specific *arr3a* (red) shows that *samd7* is expressed in immature *arr3a*$^{-}$ photoreceptors ("immature photoreceptors"). (*D*) Whole-mount view of the eye in *C*. (*E*) Close-up view of the dotted square in *D* shows *samd7*$^{+}$ puncta in *arr3a*$^{+}$ red and green cone cell bodies. (*F*) Optical cross-section of the peripheral larval retina stained with probes against *samd7* (green) and blue/UV-cone-specific *arr3b* (red). (*G*) Whole-mount view of the eye in *F*. (*H*) Close-up view of the dotted square in *G* shows that *samd7* is not expressed in *arr3b*$^{+}$ blue and UV cone cell bodies. (*I*) Optical cross-section of the peripheral larval retina stained with probes against *samd7* (green) and rod-specific *gnat1* (red). (*J*) Whole-mount view of the same eye as in *I*. (*K*) Close-up view of the dotted square in *J* shows *samd7*$^{+}$ puncta in *gnat1*$^{+}$ rod cell bodies. n = 3 eyes analyzed per in situ. [Scale bar in (*C*, *D*, *F*, *G*, *I*, and *J*), 50 μm; Scale bar in (*E*, *H*, and *K*), 5 μm.] D, V, N, T: Dorsal, Ventral, Nasal, Temporal. ONH; optic nerve head. ONL; outer nuclear layer.

immature and mature photoreceptors can be readily observed in whole-mount retinal preparations (Fig. 1 *C–K*). We found that *samd7* expression is restricted to the photoreceptor layer (outer nuclear layer; ONL), confirming that *samd7* is expressed exclusively in photoreceptors (Fig. 1 *C*, *F*, and *I*). We also observed *samd7* expression in the dorsal retina, where photoreceptors have yet to initiate *arr3a* and *arr3b* expression, indicating that *samd7* is expressed in immature photoreceptors (Fig. 1 *C* and *F*). To define the mature photoreceptor subtypes in which *samd7* is expressed, we evaluated *samd7* coexpression in *arr3a*$^{+}$ green and red cones, *arr3b*$^{+}$ UV and blue cones, and *gnat1*$^{+}$ rods. We found *samd7* to be expressed in *arr3a*$^{+}$ green and red cones (Fig. 1 *D*, *Inset*; Fig. 1*E*) and excluded from *arr3b*$^{+}$ UV and blue cones (Fig. 1 *G*, *Inset*; Fig. 1*H*). In addition, we found *samd7* to be expressed in *gnat1*$^{+}$ rods (Fig. 1 *J*, *Inset*; Fig. 1*K*). These results demonstrate that *samd7* is expressed in immature photoreceptors, red cones, green cones, and rods at larval stages.

Loss of *samd7* Results in Subtype-Specific Changes in Photoreceptor Gene Expression. To elucidate the role of *samd7* in zebrafish photoreceptor development, we engineered a mutation in the gene. Using CRISPR-Cas9 technology, we created a 10 bp deletion in the fourth exon of *samd7*, which is predicted to result in a frameshift and premature stop codon upstream of the SAM domain (*SI Appendix*, Fig. S2). To evaluate the mutation's effects on gene expression, we performed RNA-seq on the eyes of clutch-matched 5-dpf *samd7*$^{-/-}$ and wild-type (WT) control larvae. We found that only 90 genes were significantly dysregulated in the *samd7*$^{-/-}$ eye compared to controls (p-adj < 0.05; Dataset S1). We first focused on changes in red cone, green cone, and rod gene expression since these are the cell types in which *samd7* is expressed. Strikingly, we observed a nearly complete loss of green opsin (both larva-expressed green opsin paralogs, *opn1mw1* and *opn1mw2*, are absent) (41) as well as loss of the red/green-cone-specific cone arrestin, *arr3a* (5) (Fig. 2 *A* and *C* and Dataset S1). These findings suggest that green cones are absent from the eye of *samd7*$^{-/-}$ larvae. Aside from loss of *arr3a* expression, we observed only subtle changes in red-cone-specific gene expression. Specifically, we saw an ~twofold reduction in red-cone-specific *si:busm1-57f23.1* (5, 14) transcripts and a sixfold increase in *opn1lw1,* one of the two tandemly arrayed zebrafish red opsin paralogs (6) (Fig. 2 *B* and *C*).

In addition to these changes, we observed a striking reduction in rod-specific gene expression (Fig. 2*B*). Among the 66 significantly down-regulated genes in the mutant eye, 28 were rod-enriched. On average, the expression of individual rod genes was reduced by ~70% in the mutant eyes (Dataset S1).

We also observed an increase in blue- and UV-cone-specific gene expression in the *samd7*$^{-/-}$ eye. Among blue cone-specific genes, we detected an increase in blue cone opsin (*opn1sw2*) expression, as well as a corresponding increase in *foxq2*, a TF required for blue cone fate specification (11) (Fig. 2 *B* and *C*). Among UV cone-specific gene expression changes, we observed an increase in *tbx2a,* a TF that regulates the expression of UV cone opsin (*opn1sw1*) (4). There was also a suggestion of increased *opn1sw1* expression in the mutant, but this change was not statistically significant (p-adjusted = 0.07) (Fig. 2 *B* and *C* and Dataset S1). We also observed an increase in *arr3b* and *skor1a,* which are coexpressed in both blue and UV cones (4, 5) (Fig. 2*B*). Overall, the increases in blue and UV-cone-specific gene expression ranged from 1.5 to 2-fold (Dataset S1), suggesting that the total number of blue and UV cones may be increased by a corresponding amount. We also observed an increase in the expression of *exorh*, a homolog of *rho* normally restricted to a subset of photoreceptors in the zebrafish pineal gland (42) (Fig. 2 *B* and *C*). We found that *samd7* transcript levels are also increased in the *samd7*$^{-/-}$ eye, raising the possibility that Samd7 represses its own expression (Fig. 2*B*).

Loss of *samd7* Causes Changes in Photoreceptor Cell Fate. To determine whether the changes in gene expression in the *samd7*$^{-/-}$ retina are due to changes in the proportions of photoreceptor types, we used a combination of antibody staining and transgenic reporter expression to quantify rods and cone subtypes in 5-dpf clutch-matched *samd7*$^{-/-}$ and WT zebrafish. We found that there were approximately twice as many UV opsin^{+} outer segments in the central retina of *samd7*$^{-/-}$ compared to WT (Fig. 3 *A–E*). Similarly, we found about twice as many blue opsin^{+} outer segments in the central retina of *samd7*$^{-/-}$ compared to WT (Fig. 3 *F–J*). The increase in UV and blue opsin^{+} cells is commensurate with the ~twofold increase in UV and blue cone-specific gene expression in the *samd7*$^{-/-}$ eye (Fig. 2 *B* and *C* and Dataset S1). We were unable to detect any green opsin^{+} outer segments in the *samd7*$^{-/-}$ retina (Fig. 3 *K–O*),

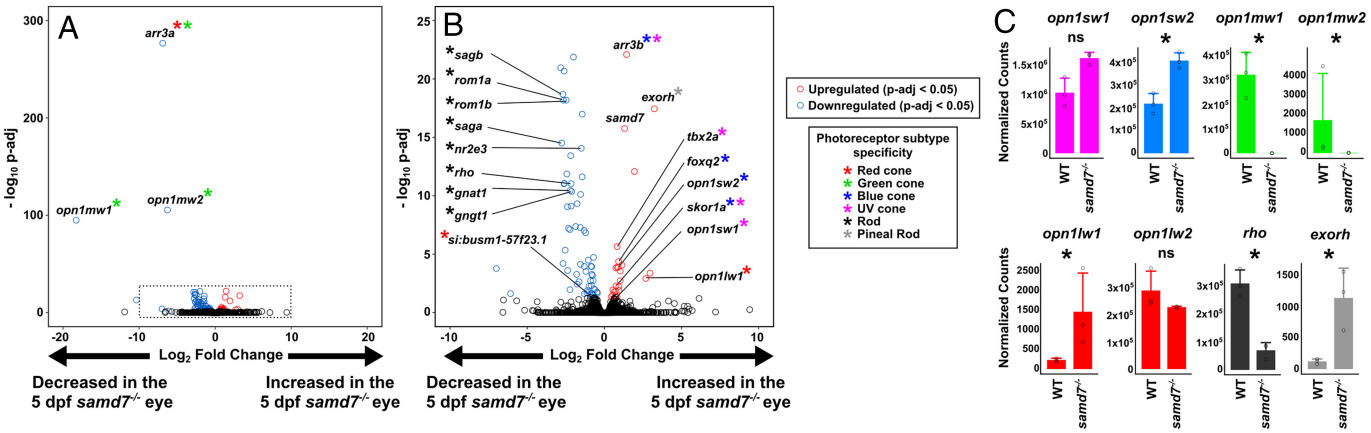

Fig. 2. Rod- and green cone-specific gene expression is reduced, and blue and UV-cone-specific gene expression is increased in *samd7*$^{-/-}$ eyes. (*A*) Volcano plot of bulk RNA-seq data from *samd7*$^{-/-}$ vs. WT 5-dpf eyes demonstrates a marked reduction in the expression of red/green-cone-specific *arr3a* and green-cone-specific opsins *opn1mw1* and *opn1mw2*. (*B*) A magnified view of the dotted portion of panel *A* demonstrates a marked reduction in the expression of multiple rod-specific genes, a subset of which are annotated. The expression of multiple blue and UV cone-specific genes is increased in the mutant, including blue/UV-cone-specific *arr3b* and blue opsin (*opn1sw2*). UV opsin (*opn1sw1*) appeared somewhat increased, but the change is not statistically significant (p-adj = 0.07, Dataset S1). Among red-cone-specific genes, *si:busm1-57f23.1* is decreased, and *opn1lw1* is increased. *Exorh,* which is normally restricted to a subset of pineal photoreceptors, is also increased (42). (*C*) Bar plots of opsin expression (DESeq2-normalized counts) from RNA-seq data in panels *A* and *B* (mean ± SD; n = 3 per group) *p-adj < 0.05. ns, not significant. SD, standard deviation.

consistent with the lack of green opsin expression we observe in the mutant eye by RNA-seq (Fig. 2*A* and Dataset S1). The number of red cones (*thrb:tdTomato*$^+$) was unchanged in the mutant (Fig. 3 *P*–*T*).

To evaluate changes in the number of rods in *samd7*$^{-/-}$ larvae, we characterized the distribution of Gnat1$^+$ cells in the retina. In WT retina, Gnat1$^+$ rods are highly concentrated in the ventral-most region and more sparsely distributed throughout other regions (Fig. 3*U*). In the *samd7*$^{-/-}$ retina, Gnat1$^+$ cells were absent from all regions except the ventral-most retina, in which the intensity of Gnat1 labeling was reduced relative to WT (Fig. 3*V*). This severe reduction in the number of Gnat1$^+$ rods correlates with the ~80% reduction in *gnat1* expression we observe in the *samd7*$^{-/-}$ eye (Fig. 2*B* and Dataset S1). To determine whether cell death might account for the reduction in rods at 5-dpf, we characterized *rho:GFP* expression in clutch-matched *samd7*$^{-/-}$ and WT zebrafish at 3-dpf, the earliest time point at which rods can be observed throughout the larval retina (43). We found that at 3-dpf the majority of rods (*rho:GFP*$^+$) are already absent from the central and dorsal *samd7*$^{-/-}$ retina, although the ventral patch of rods remains (*SI Appendix*, Fig. S3 *A* and *B*). These results suggest that rods fail to be born in the *samd7*$^{-/-}$ retina. To determine whether the remaining population of ventral rods might be transformed into hybrid rod/UV cones, as occurs in the *Samd7*$^{-/-}$ mouse retina, we stained 5-dpf WT;*rho:GFP*$^+$ and *samd7*$^{-/-}$;*rho:GFP*$^+$ eyes for UV opsin (38). We found that neither WT nor *samd7*$^{-/-}$ rods express UV opsin (*SI Appendix*, Fig. S3 *C*–*J*). Taken together, our results suggest that the vast majority of rods fail to differentiate at 3-dpf and that the remaining ventral population does not adopt a rod/UV-hybrid phenotype, in contrast to the hybrid phenotype observed in *Samd7*$^{-/-}$ mouse rods (38). However, it remains possible that some rod precursors are transfated to UV cones in the central/dorsal *samd7*$^{-/-}$ retina, but are undetectable with available rod-specific markers.

In summary, we find that both the number of UV opsin$^+$ and blue opsin$^+$ cones are approximately doubled, green opsin$^+$ cones are absent, the number of red cones is unchanged, and the number of rods is severely reduced in the *samd7*$^{-/-}$ retina. Next, we sought to determine the identity of the supernumerary UV opsin$^+$ cells in the *samd7*$^{-/-}$ retina. Based on the expression of *samd7* in red cones, green cones, and rods, we hypothesized that loss of *samd7* could result in the upregulation of UV opsin in one of these cell types. To test this hypothesis, we first characterized the expression of UV opsin in red cones (*thrb:tdTomato*$^+$ cells) in clutch-matched *samd7*$^{-/-}$ and WT 5-dpf larvae. As expected in the WT retina, we detected no UV opsin in red cones (Fig. 4*A*). In contrast, we observed strong UV opsin staining in *samd7*$^{-/-}$ red cones (Fig. 4*B*). Similarly, *opn1sw1:GFP*$^+$, a UV-cone-specific transgene, was up-regulated in nearly all red cones in the *samd7*$^{-/-}$ retina (Fig. 4 *C* and *D*). These results suggest that red cones are transformed into hybrid red/UV cones in the *samd7*$^{-/-}$ retina. When red-cone-derived UV cones (*thrb:tdTomato*$^+$;*opn1sw1:GFP*$^+$) are excluded from our analysis, we still observe a statistically significant increase in the number of UV cones in the *samd7*$^{-/-}$ retina (Fig. 4*E*), suggesting that a small subset of supernumerary UV cones in the *samd7*$^{-/-}$ retina derive from another unknown cell type.

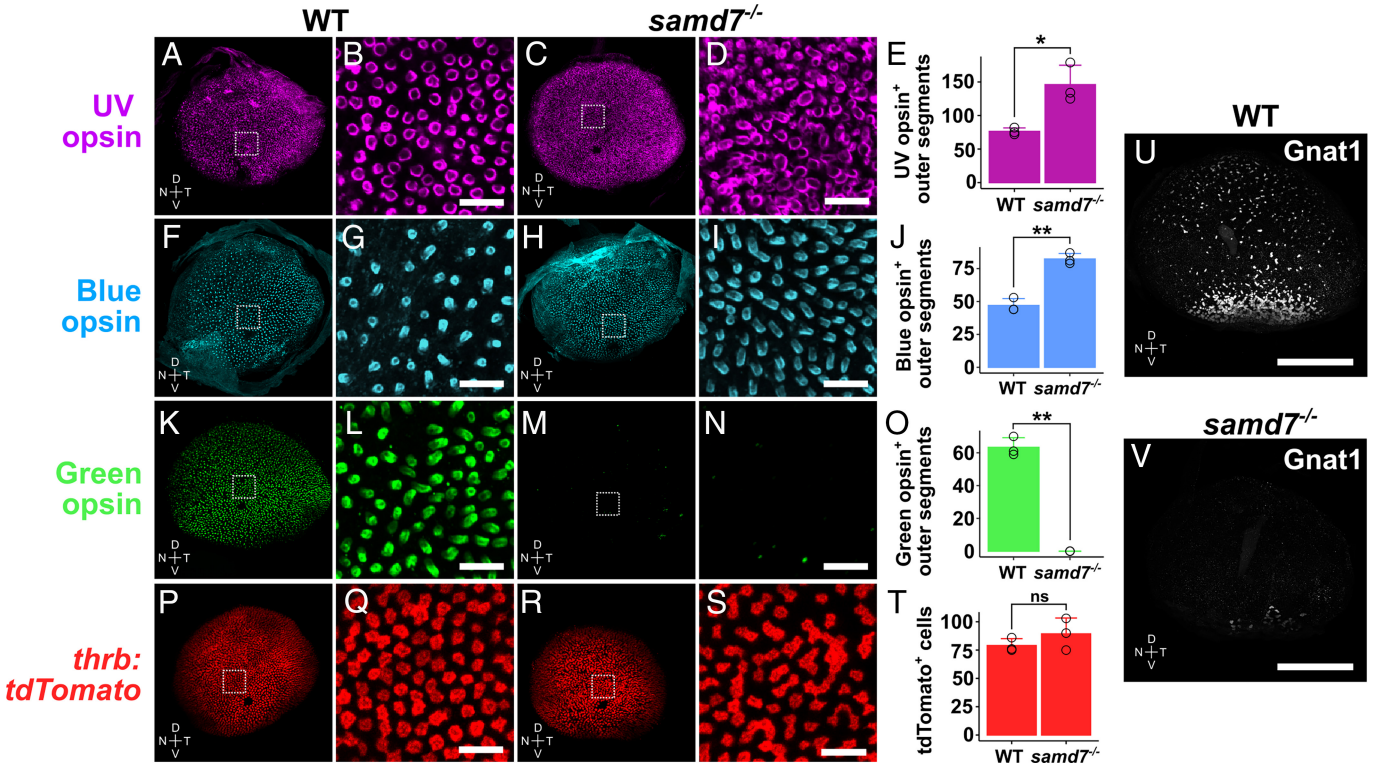

Fig. 3. The numbers of blue and UV cones are approximately doubled, whereas green cones and rods are severely reduced in *samd7*$^{-/-}$ larvae. Confocal whole-mount images and high magnification *insets* of 5-dpf WT and *samd7*$^{-/-}$ eyes. (*A*–*E*) The number of UV cones stained with the UV opsin antibody is approximately doubled. (*F*–*J*) The number of blue cones stained with the blue opsin antibody is approximately doubled. (*K*–*O*) Green cones, as stained with the green opsin antibody, are absent from the *samd7*$^{-/-}$ eye. (*P*-*T*) The number of red cones, as identified with the *thrb:tdTomato* transgene, is unchanged, although the percentage of red cones that are directly contiguous appears to be increased in the mutant. (*U* and *V*) There is a severe reduction in the number of rods stained with the Gnat1 antibody, although a small population of rods with reduced Gnat1 signal can be observed in the ventral *samd7*$^{-/-}$ retina. (mean ± SD; n = 3 per group). All fields of view quantified in (*E*, *J*, *O*, and *T*) were 40 × 40 μm^2. Scale bars in all close-up views (*B*, *D*, *G*, *I*, *L*, *N*, *Q*, and *S*) = 10 μm. [Scale bar in (*U* and *V*), 100 μm.] D, V, N, T: Dorsal, Ventral, Nasal, Temporal. Statistical comparisons were performed using the two-tailed, unpaired *t* test assuming unequal variance. *P < 0.05, **P < 0.005. ns, not significant. SD, SD.

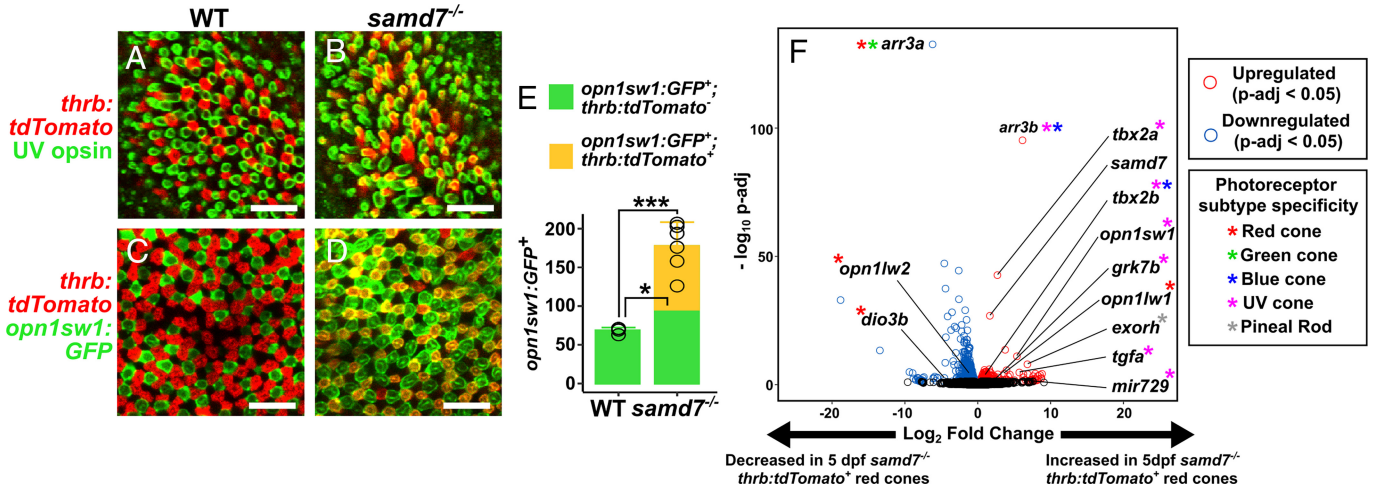

Fig. 4. Red cones are transformed into hybrid red/UV cones in the larval *samd7*$^{-/-}$ retina. (*A–D*) Confocal images of 5-dpf WT and *samd7*$^{-/-}$ eyes show that UV opsin and UV-cone-specific *opn1sw1:GFP* is up-regulated in *samd7*$^{-/-}$ red cones (*thrb:tdTomato*$^{+}$). (*E*) UV cones (*opn1sw1:GFP*$^{+}$ cells per 1,600 μm^2) are increased in the *samd7*$^{-/-}$ retina. The subset of UV cones that are not derived from red cones (*opn1sw1:GFP*$^{+}$*;thrb:tdTomato*$^{-}$) are also increased, suggesting that a small subset of supernumerary UV cones in the *samd7*$^{-/-}$ retina derive from another unknown cell type or precursor (mean ± SD; n = 4 WT, n = 6 *samd7*$^{-/-}$). (*F*) Volcano plot from bulk RNA-seq comparing gene expression in isolated 5-dpf WT *thrb:tdTomato*$^{+}$ cells (i.e., red cones) and *samd7*$^{-/-}$ *thrb:tdTomato*$^{+}$ cells (i.e., transformed hybrid red/UV cones). UV-cone genes are up-regulated in *samd7*$^{-/-}$ hybrid red/UV cones including *tbx2a, tbx2b, opn1sw1, arr3b, mir729, tgfa,* and *grk7b* (5). Red-cone-specific changes in gene expression were also observed, including reduced expression of the thyroid-hormone-inactivating enzyme, *dio3b;* increased expression of the red-shifted red opsin paralog, *opn1lw1* (λ_{max} = 558 nm); and decreased expression of the blue-shifted red opsin paralog, *opn1lw2* (λ_{max} = 548 nm). Similar changes in red opsin paralog expression were previously observed in larval zebrafish treated with thyroid hormone (44). Red/green-cone-specific *arr3a* expression was absent, and *exorh* and *samd7* expression were increased in *samd7*$^{-/-}$ hybrid red/UV cones. (Scale bar, 10 μm.) Statistical comparisons in *E* were performed using the two-tailed, unpaired *t* test assuming unequal variance. *P < 0.05 and ***P < 0.0005. SD, standard deviation.

To evaluate the possibility that the supernumerary blue opsin^{+} cells observed in *samd7*$^{-/-}$ retina might represent hybrid blue/red cones, we characterized the expression of blue opsin and blue-cone-specific *opn1sw2:GFP* in red cones (*thrb:tdTomato*$^{+}$) of WT and *samd7*$^{-/-}$ larvae (45). As expected, we found a near doubling of the number of *opn1sw2:GFP*$^{+}$ cells in the *samd7*$^{-/-}$ retina (*SI Appendix*, Fig. S4*E*), consistent with the results of blue opsin antibody staining (Fig. 3 *F–J*). However, we found that neither blue opsin nor the *opn1sw2:GFP* transgene are expressed in red cones in the *samd7*$^{-/-}$ retina (*SI Appendix*, Fig. S4 *A–D*), suggesting that supernumerary blue cones are not derived from red cones but may instead arise from another population of *samd7*$^{+}$ photoreceptors, possibly transfated rods or green cones.

RNA-seq Reveals Hybrid Red/UV Cones in the *samd7*$^{-/-}$ Retina. To further evaluate gene expression changes in *samd7*$^{-/-}$ red cones, we used FACS to isolate red cones (*thrb:tdTomato*$^{+}$ cells) from the eyes of 5-dpf *samd7*$^{-/-}$ and WT larvae and compared their transcriptomes by RNA-seq. As expected, we observed an upregulation of UV opsin (*opn1sw1*) in *samd7*$^{-/-}$ red cones relative to WT (Fig. 4*F*). In addition, we saw upregulation of *mir729, tgfa, tbx2a,* and *grk7b,* which were previously shown to be UV-cone-enriched in adult zebrafish photoreceptors (4, 5) (Fig. 4*F*). We also observed an increase in *tbx2b,* a UV/blue-cone-enriched transcription factor (4, 5). Both *tbx2a* and *tbx2b* had previously been shown to regulate *opn1sw1* expression in UV cones (4, 11, 12). We did not detect upregulation of the blue-cone-specific genes *opn1sw2* and *foxq2* in *samd7*$^{-/-}$ red cones (Dataset S2). These results support the conclusion that red cones are transformed into hybrid red/UV cones in the *samd7*$^{-/-}$ retina.

We also observed dysregulation of several red-cone-specific genes in *samd7*$^{-/-}$ red cones. Red/green-cone-specific *arr3a* transcripts are essentially absent. In addition, the expression of *opn1lw2* [λ_{max} = 548 nm (6)], the predominant red cone opsin transcript in WT larvae, is reduced; whereas the expression of *opn1lw1* [λ_{max} = 558 nm (6) is correspondingly increased (Fig. 4*F* and Dataset S2). A similar decrease in *opn1lw2* and increase in *opn1lw1* was previously observed in zebrafish larvae treated with thyroid hormone (44). Therefore, we hypothesized that thyroid hormone signaling was increased in *samd7*$^{-/-}$ red cones. Consistent with this hypothesis, we observed a decrease in the expression of the thyroid-hormone-inactivating enzyme *dio3b* in *samd7*$^{-/-}$ red cones (46) (Fig. 4*F* and Dataset S2). This decrease in *dio3b* may result in elevated levels of active thyroid hormone, thereby mimicking changes in *opn1lw1/2* paralog expression observed in larvae treated with thyroid hormone. Previous reports also showed that application of thyroid hormone reduced *si:busm1-57f23.1* expression, consistent with the reduction in this gene's expression which we observed in *samd7*$^{-/-}$ whole eye by RNA-seq (Fig. 2*B* and Dataset S1) (47).

We also detect a reduction in green opsin (*opn1mw1/2)* expression in *samd7*$^{-/-}$ red cones (Dataset S2), which we attribute to trace (~4%) contamination of green cones in the WT sorted cells, as detailed in the Methods section. In summary, we find that UV-cone-specific gene expression is up-regulated in *samd7*$^{-/-}$ red cones, while blue cone-specific-gene expression (i.e., *foxq2* and *opn1sw2*) is unchanged (Fig. 4*F* and Dataset S2). In addition, we find that thyroid hormone signaling may be increased, resulting in increased *opn1lw1* and reduced *opn1lw2* expression (Fig. 4*F*).

The Adult *samd7*$^{-/-}$ Retina Recapitulates Aspects of the Larval Phenotype and Demonstrates a Reduced Electrical Response to Light. To determine whether the function of *samd7* in the adult retina is similar to that in the larval retina, we isolated retinas from 3-mo-old *samd7*$^{-/-}$ and WT zebrafish and compared their transcriptomes by RNA-seq. We find changes in gene expression similar to those we observed in the *samd7*$^{-/-}$ larvae, with some notable exceptions. Consistent with the larval phenotype, we observe a near absence of all green opsin transcripts (*opn1mw1/2/3/4*) as well as loss of red/green-cone-specific *arr3a* from the adult *samd7*$^{-/-}$ retina, suggesting that green cones are absent (*SI Appendix*, Fig. S5*A* and Dataset S3). We also observe an increase in blue and UV-cone-specific gene expression. Among blue-cone-specific genes, we observe a 1.7-fold increase in *foxq2* and a 1.9-fold increase in blue opsin (*opn1sw2*). Similarly, we find that UV-cone-specific gene expression is increased in the adult

mutant retina; *opn1sw1, mir729, tbx2a,* and *tgfa* transcript levels are all increased between twofold and fourfold (*SI Appendix*, Fig. S5*A* and Dataset S3). We also see an increase in *exorh* expression, as seen in the larval *samd7*$^{-/-}$ eye (Fig. 2*B*, *SI Appendix*, Fig. S5*A*, and Datasets S1 and S3). As in larvae, these changes are consistent with an absence of green cones and increased numbers of blue cones in the mutant, as well as upregulation of UV-cone-specific genes in red cones.

Among red-cone-enriched genes, we find that one red cone opsin paralog (*opn1lw2*) is reduced by ~97% while the second (*opn1lw1*) is unchanged in the adult *samd7*$^{-/-}$ retina compared to WT (*SI Appendix*, Fig. S5*A* and Dataset S3). Transcripts of red-cone-specific *thrb, si:busm1-57f23.1,* and *mir726* are also reduced (*SI Appendix*, Fig. S5*A* and Dataset S3). Although red-cone-specific gene expression is generally reduced, the sustained expression of *opn1lw1* and the concurrent increase in UV-cone-specific gene expression suggests that red cones assume a hybrid red/UV-cone phenotype, as we observe in the larval *samd7*$^{-/-}$ retina (Fig. 4 *A–D*). In contrast to the larval phenotype, we do not observe downregulation of rod-specific-phototransduction components in the adult *samd7*$^{-/-}$ retina, with the exception of *saga* (*SI Appendix*, Fig. S5*A* and Dataset S3). However, we do observe a reduction in *nrl* expression by ~60%. We also find an adult rod-enriched gene, *ppdpfa*, a putative signaling molecule of unknown function (5, 48), to be reduced by ~60% (*SI Appendix*, Fig. S5*A* and Dataset S3). Conversely, we find that *mafba,* a TF recently shown to regulate rod specification in conjunction with *nrl* in the adult zebrafish retina (9), to be increased by ~twofold (*SI Appendix*, Fig. S5*A* and Dataset S3). Overall, we find that the changes in rod gene expression in the mutant adult retina and larval eye are distinct; although rod genes represent about half of the dysregulated genes in the larval mutant dataset (Dataset S1), very few of the dysregulated genes we observe in the adult dataset are rod-specific (*SI Appendix*, Fig. S5*A* and Dataset S3). These differences may reflect the distinct developmental origin of the embryonic vs. adult zebrafish retina and the apparent differences in the requirement of *nrl* in the specification of larval and adult rods (8, 9, 49). Thus, *samd7* appears to play distinct gene regulatory roles in mediating rod gene expression in the larval vs. adult retina.

Strikingly, we also observed upregulation of a subset of genes associated with Müller-glia-mediated regeneration in the adult *samd7*$^{-/-}$ retina. In response to some types of retinal injury, Müller glia reenter the cell cycle, proliferate, and give rise to new neurons, including both rods and cones (50). In the adult *samd7*$^{-/-}$ retina, we see an increase in the expression of TFs *ascl1a* and *insm1a* (*SI Appendix*, Fig. S5*A* and Dataset S3), which were previously shown to be up-regulated in Müller glia during regeneration and required for the regenerative response (51, 52). We also observed upregulation of genes involved in the cell cycle, including cyclin D1 (*ccnd1*), *cdk1* (cyclin-dependent kinase 1), and *mki67* (a marker of proliferation). Finally, we observe an increase in *prdm1a*, a TF expressed transiently in immature photoreceptors (39, 40) (*SI Appendix*, Fig. S5*A* and Dataset S3). These data suggest that in the adult *samd7*$^{-/-}$ retina, Müller glia up-regulate genes associated with regeneration, proliferation, and the birth of new photoreceptors, perhaps in response to ongoing photoreceptor loss.

In the adult zebrafish retina, cone photoreceptors are arranged in a highly regular "row mosaic" in which a single row of UV and blue cones alternates with double rows of red and green cones (49). To evaluate changes in the mosaic in *samd7*$^{-/-}$ retina, we compared retinal flat-mount preparations from adult *samd7*$^{-/-}$ and WT fish which were stained with antibodies against Arr3a [a marker of red and green cones (53)] and Arr3b [a marker of UV and blue cones (54)]. In WT retina, we observed the regular mosaic arrangement of photoreceptors: double rows of Arr3a^{+} red and green cones alternating with a single row of Arr3b^{+} blue and UV cones (*SI Appendix*, Fig. S5*B*). In contrast, *samd7*$^{-/-}$ retinas show a severe disruption of the photoreceptor mosaic, including a disordered arrangement of Arr3b^{+} cells and a complete absence of Arr3a^{+} cells (*SI Appendix*, Fig. S5*C*). The latter finding is consistent with the loss of *arr3a* expression we observed by RNA-seq analysis (*SI Appendix*, Fig. S5*A* and Dataset S3).

To determine whether rod and cone photoreceptor function is affected in *samd7*$^{-/-}$ fish, we performed ex vivo electroretinogram (ERG) recordings of adult *samd7*$^{-/-}$ and WT retinas. First, we measured the response of rods to 530 nm flashes of increasing intensity under scotopic conditions. Next, we measured the response of cones to 448, 530, and 655 nm flashes of increasing intensity. These wavelengths are expected to stimulate distinct subsets of cone opsins (*SI Appendix*, Fig. S6*A* and Table S1). We find that the maximal response amplitude (R_{max}) is significantly reduced in rods, and in cones stimulated at 530 and 655 nm (*SI Appendix*, Fig. S6 *B*, *D*, and *E* and Table S1). We also detected a possible reduction of R_{max} in cones stimulated at 448 nm, but the effect was not statistically significant (P = 0.09; *SI Appendix*, Fig. S6*C* and Table S1). Response kinetics do not appear to be significantly affected in any of the rod or cone stimulating conditions (*SI Appendix*, Fig. S6 *F–I*).

The rod ERG response is reduced despite the fact that we observed very few changes in rod-specific gene expression by RNA-seq in the adult retina (*SI Appendix*, Figs. S5*A* and S6*B* and Dataset S3). The reduction of the ERG response to 448 and 530 nm stimuli (*SI Appendix*, Fig. S6 *C* and *D*) is consistent with the absence of green opsin expression in the adult *samd7*$^{-/-}$ retina (*SI Appendix*, Fig. S5*A* and Dataset S3), because both 448 and 530 nm stimuli are within the range of green opsin absorbances (*SI Appendix*, Fig. S6*A*). However, we do observe a trend in the increase of the normalized 448 nm response (absolute amplitude normalized to maximum response amplitude) in the *samd7*$^{-/-}$ retina (*SI Appendix*, Fig. S6 *C*, *Inset*), suggesting there may be a relative gain in the contribution of blue cones in the mutant retina, consistent with increased blue opsin expression (*opn1sw2*) (*SI Appendix*, Fig. S5*A* and Dataset S3). We also observe a reduction in the red-cone ERG response to 655 nm stimuli (*SI Appendix*, Fig. S6*E*), consistent with the reduction in the expression of red opsin (*opn1lw2*) in the *samd7*$^{-/-}$ retina (*SI Appendix*, Fig. S5*A* and Dataset S3). Taken together, these experiments reveal an across-the-board reduction in the absolute rod and cone electrical responses and a potential increase in the relative responses of blue cones in the adult *samd7*$^{-/-}$ retina, consistent with the observed changes in expression of opsins and other phototransduction components.

Samd7 Represses S-Opsin Expression in Dorsal M-Cones of the Mouse Retina. In the *samd7*$^{-/-}$ zebrafish retina, red cones are transformed into hybrid red/UV cones in which both red (*opn1lw1*) and UV opsin (*opn1sw1*) are coexpressed (Fig. 4 *B* and *F*). In the WT mouse retina, M-cones in the ventral zone show a strikingly similar phenotype: coexpression of M- and S-opsin (36). Since mouse M- and S-opsins are orthologous to zebrafish red and UV cone opsins, respectively, we hypothesized that the upregulation of S-opsin in these cells could be the result of reduced *Samd7* expression (7). Indeed, a recent study found that *Samd7* expression was reduced in ventral mouse cones compared to dorsal (55). To further evaluate our hypothesis, we engineered *Samd7*$^{-/-}$ mice (*Materials and Methods* and *SI Appendix*, Fig. S2) and performed antibody staining for M- and S-opsin on flat-mount preparations of adult WT and *Samd7*$^{-/-}$ retina. We found that in the WT retina, M-opsin is enriched in the dorsal retina and S-opsin is enriched in the central/ventral retina, as previously reported (36) (Fig. 5 *A–C*). In the *Samd7*$^{-/-}$ retina, we found that S-opsin expression was markedly up-regulated throughout the dorsal retina (Fig. 5*D*).

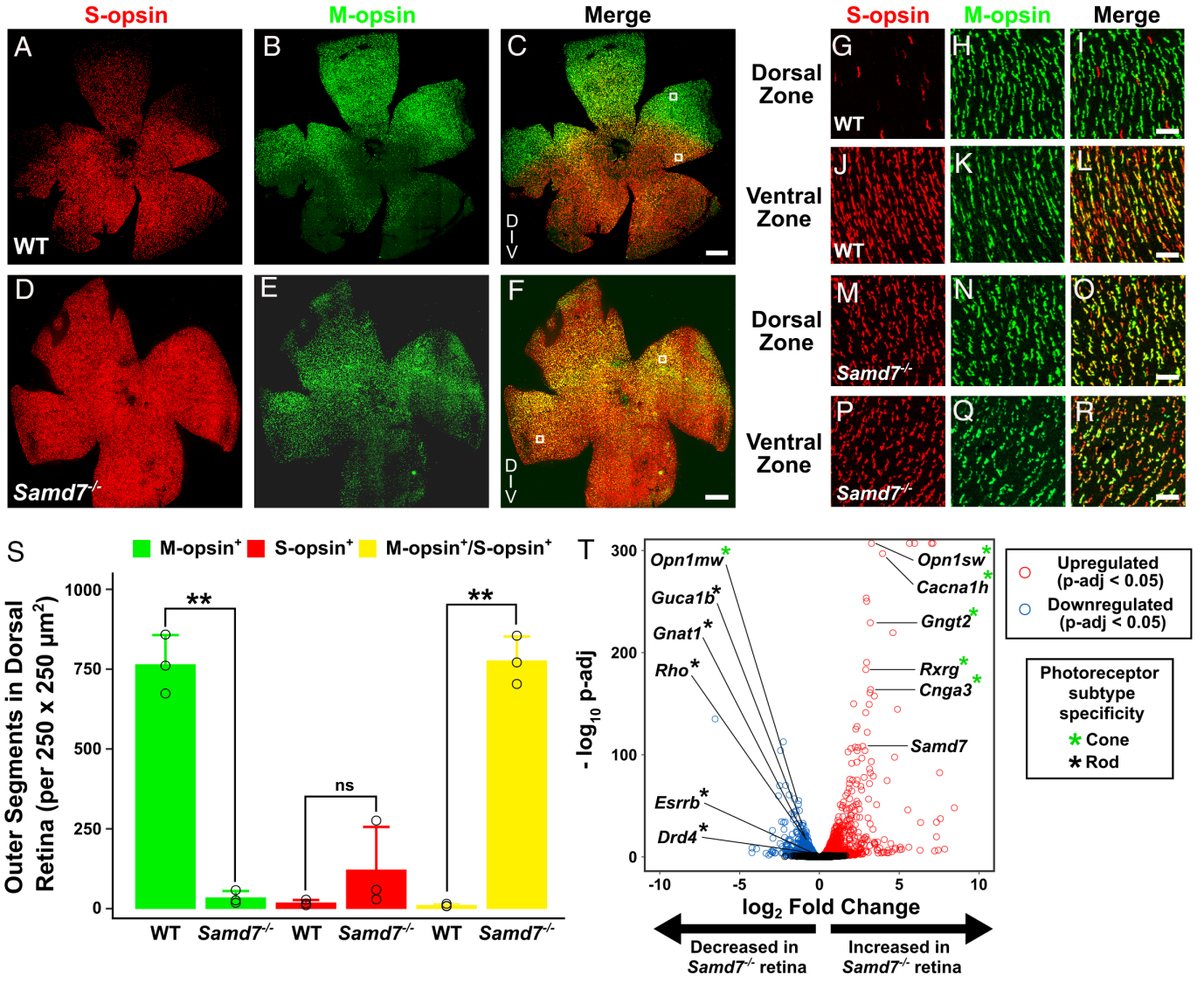

Fig. 5. Dorsal M-cones are transformed into hybrid M/S-cones in the mouse *Samd7*$^{-/-}$ retina. (*A–F*) Flat mounts of adult WT and *Samd7*$^{-/-}$ mouse retina stained with S- and M-opsin antibodies demonstrate that S-opsin signal is increased throughout the dorsal region of *Samd7*$^{-/-}$ retina. (*G–R*) Close-up views of boxed *insets* from panels *C* and *F* reveal that S-opsin is up-regulated specifically in dorsal *Samd7*$^{-/-}$ M-opsin^{+} cones (i.e., M-cones are transformed into hybrid M/S-opsin^{+} cones). (*S*) The number of exclusively M-opsin^{+} cones in the dorsal *Samd7*$^{-/-}$ retina is reduced to a similar degree as the increase in the number of mixed M/S-opsin^{+} cones, supporting the conclusion that M-cones are transformed into hybrid M/S-opsin^{+} cones (mean ± SD; n = 3/genotype). (*T*) RNA-seq analysis of WT and *Samd7*$^{-/-}$ mouse retina demonstrates a reduction in rod-specific gene expression and an increase in cone-specific gene expression, with the exception of M-opsin (*Opn1mw*), which is somewhat reduced. Labeled genes were previously found to be dysregulated by qPCR analysis in another *Samd7* mutant (38). Genes touching the top edge of the Volcano plot (e.g., *Opn1sw*) have p-adjusted values equal to zero (n = 3 retinas/genotype). *Samd7*^{minus19A} mutants were used for flat-mount imaging and quantification in panels *A–S*. *Samd7*^{minus10A} mutants were used for RNA-seq in panel *T*. [Scale bar in (*A–F*), 500 µm; Scale bar in (*G–R*), 20 µm.] D, V: Dorsal, Ventral. Statistical comparisons in *S* were performed using two-tailed, unpaired *t* test assuming unequal variance. $^{**}P < 0.005$. SD, standard deviation.

Closer inspection of individual outer segments in the *Samd7*$^{-/-}$ retina revealed that all dorsal M-opsin^{+} cones coexpress S-opsin (Fig. 5 *M–O*), in contrast to the WT retina in which dorsal M-opsin^{+} cones largely lack S-opsin (Fig. 5 *G–I*). Quantitative analysis revealed a severe reduction in the number of M-opsin-only cones in the dorsal *Samd7*$^{-/-}$ retina and a corresponding increase in the number of M- and S-opsin coexpressing cones (Fig. 5*S*). We conclude that *Samd7* is required for the repression of S-opsin in dorsal M-cones.

To further analyze the *Samd7* mutant phenotype, we performed RNA-seq analysis on WT and *Samd7*$^{-/-}$ retina of adult mice in three biological replicates. We found that 195 genes were significantly dysregulated by >twofold in the *Samd7*$^{-/-}$ retina (Dataset S4). A much larger number of genes were more subtly dysregulated (i.e., <twofold; Dataset S4). As previously reported, we saw upregulation of a subset of cone genes (including *Opn1sw*) and downregulation of a subset of rod genes (including *Rho* and *Gnat1*) (38). Our findings are fully concordant with the expression changes verified by qPCR in a prior study of *Samd7*$^{-/-}$ mouse retina, with the exception of M-opsin (*Opn1mw*), which we find to be reduced by ~60% in our mutant (Fig. 5*T* and Dataset S4) (38). We also found that *Samd7* transcript levels are increased in the *Samd7*$^{-/-}$ retina, raising the possibility that Samd7 represses its own expression (Fig. 5*T* and Dataset S4), similar to our observations in zebrafish (Fig. 2*B*).

Discussion

In the present study, we identify key roles for *samd7* in preserving normal rod and cone photoreceptor identity in zebrafish and mice. In the zebrafish *samd7*$^{-/-}$ retina, we found that red cones are transformed into hybrid red/UV cones, green cones are absent, the number of blue cones is approximately doubled, and the number of rods is greatly reduced (Fig. 6). These diverse phenotypes

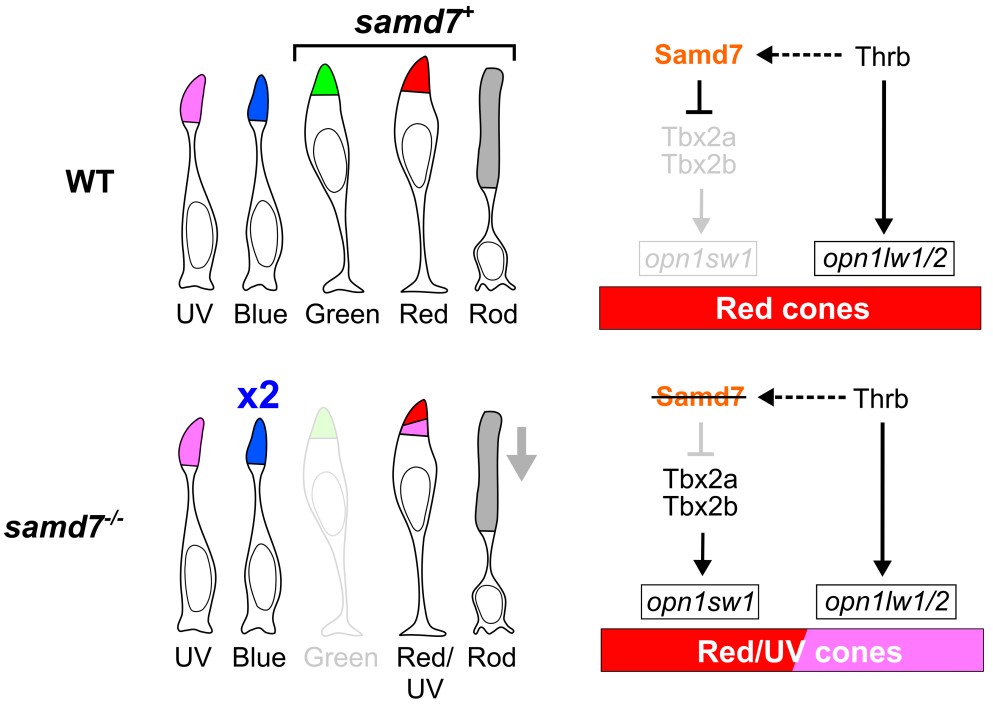

Fig. 6. The role of *samd7* in zebrafish photoreceptor specification. Diagram of cone subtypes in the WT and *samd7*$^{-/-}$ zebrafish retina. In the *samd7*$^{-/-}$ retina, red cones are transformed into hybrid red/UV-sensitive cones, green cones are absent, blue cones are approximately doubled, and the number of rods is greatly reduced. We propose that Samd7 represses UV-cone-specific gene expression by repressing *tbx2a* and *tbx2b,* two key regulators of *opn1sw1* expression (4, 11, 12) Activation is indicated with an arrowhead, and repression with a flat bar. Black coloring indicates that the factor is expressed, and gray indicates that it is not. A dashed line represents a proposed regulatory relationship and a solid line represents a previously verified regulatory function.

suggest that *samd7* mediates distinct functions in individual photoreceptor types. Loss of green cones and a concomitant increase in the number of blue cones might be explained by direct transfating of green cones into blue cones in the *samd7*$^{-/-}$ background. Alternatively, supernumerary blue cones could originate from another population of *samd7*$^{+}$ precursors, such as those that normally give rise to rods. Future lineage-tracing experiments will be required to test these ideas. We also found a role for *samd7* in zebrafish red cones. In the *samd7*$^{-/-}$ retina, red cones up-regulate multiple UV-cone genes while maintaining expression of red-cone genes. In contrast, in the *thrb*$^{-/-}$ retina, red cones are completely transfated into UV cones (13, 14). We therefore propose that *thrb* regulates red cone identity via two distinct mechanisms: 1) direct activation of red-cone genes and 2) repression of UV-cone genes via induction of *samd7* expression (Fig. 6).

In the *Samd7*$^{-/-}$ mouse retina, we observed S-opsin upregulation in dorsal M-cones, analogous to the upregulation of UV opsin in zebrafish *samd7*$^{-/-}$ red cones. A similar phenotype has also been reported in other mouse mutants (28–30, 34, 35), suggesting that *Samd7* may be part of a regulatory network required to repress S-opsin dorsally. *SAMD7* is also enriched in long-wavelength-sensitive cones in chickens and humans (56–58), and human patients with *SAMD7* mutations display selective degeneration of the cone-rich macula (59). Thus, *SAMD7* may play a role in the cones of other species, but the extent to which its function is conserved across vertebrates remains to be determined.

Materials and Methods

Animal Husbandry. All zebrafish and mouse studies were conducted in accordance with the Guide for the Care and Use of Laboratory Animals and the Animal Welfare Act and were approved by the Washington University in St. Louis Institutional Animal Care and Use Committee and by the corresponding body at the University of California, Irvine. Additional details are described in *SI Appendix, SI Materials and Methods*.

Hybridization Chain Reaction (HCR). Fluorescent in situ hybridization was performed on whole larvae according to the manufacturer's protocol (HCR v.3.0) (60). Additional details are described in *SI Appendix, SI Materials and Methods*.

Generation of *samd7* Mutant Zebrafish. Mutant zebrafish were generated using a gRNA (GGGAAGCAGAGTTGCGGCAG) targeting exon 4 of *samd7*. Additional details are described in *SI Appendix, SI Materials and Methods*.

Zebrafish Genotyping. Mutant zebrafish were genotyped by PCR using primers: 5′-GAGCTGCTTCTATTACTGACACCT-3′ and 5′-CTGCCCCTGAGCCAGGAT-3′ to detect the difference between the WT and *samd7*^{stl888} mutant allele (10 bp deletion). Additional details are described in *SI Appendix, SI Materials and Methods*.

Cell Dissociation and FACS. 5-dpf WT;*thrb:tdTomato*$^{+/-}$ and *samd7*$^{-/-}$;*thrb:tdTomato*$^{+/-}$ larval eyes were dissociated into single cells using papain (Worthington Biochem), and tdTomato^{+} cells were sorted by FACS. Additional details are described in *SI Appendix, SI Materials and Methods*.

RNA-seq. RNA was isolated, cDNA was generated, sequencing adapters were incorporated, and samples were sequenced using 150 bp paired-end reads. Additional details are described in *SI Appendix, SI Materials and Methods*.

Zebrafish Retina Immunohistochemistry and Imaging. To facilitate visualization of immunostaining patterns, larvae were treated with 200 μM N-phenylthiourea (PTU; P7629, Sigma) from 24 hpf, then killed at 5 dpf by tricaine overdose, fixed in 4% PFA with 5% sucrose overnight at 4 °C, and stored in PBS at 4 °C. Primary antibodies used were as follows: Rabbit anti-Gnat1 (1:100, SC-389, Santa Cruz), rabbit anti-green opsin [1:300, gift from David Hyde, University of Notre Dame, Notre Dame, IN (61)], rabbit anti-blue opsin (1:300, EJH012, Kerafast), rabbit anti-UV opsin (1:300, EJH013, Kerafast), mouse anti-Arr3a [1:100; mouse monoclonal zpr1 (53, 62), Zebrafish International Resource Center], Arr3b [1:100, produced at Pacific Immunology (PAC 16825-16826) by immunizing chickens with Arr3b peptide ANEEDNIDEKVEKKDTC, as previously described (54)]. Secondary antibodies used were as follows: donkey polyclonal anti-rabbit IgG conjugated with Alexa-555 (1:200; A31572, Invitrogen), donkey polyclonal anti-rabbit IgG (H^{+}L) conjugated with Alexa Fluor™ Plus 488 (1:200, A32790TR, Invitrogen), and goat polyclonal anti-chicken IgY conjugated with Alexa-488 (1:200; A11039, Invitrogen). Additional details are described in *SI Appendix, SI Materials and Methods*.

Photoreceptor Quantification in Zebrafish Larvae. For quantification of photoreceptors in the retina of 5-dpf larvae, the number of cells within a 40 × 40 μm square immediately dorsal to the optic nerve head was counted using Fiji software (63).

Transretinal ERG Recording and Analysis. Details are described in *SI Appendix, SI Materials and Methods*.

Generation of *Tg(crx:GFP)* Zebrafish, Isolation of 4-dpf *crx:GFP*$^+$ Cells, and Single-Cell RNA-seq Analysis. Details are described in *SI Appendix, SI Materials and Methods*.

***Samd7* Knockout Mouse Generation.** *Samd7* knockout mice were generated by nucleofection of C57BL/6J mouse embryos with Cas9 RNP with guide RNA targeting exon 5 of *Samd7* (CATAGAAGAGTGGTATTCCC) by the Genome Engineering and Stem Cell Center at Washington University School of Medicine (GESC). Additional details are described in *SI Appendix, SI Materials and Methods*.

Opsin Immunostaining of Retinal Flat Mounts and Quantitation. Five-week-old WT and *Samd7*$^{minus19A/minus19A}$ male mice were killed, and the sclera was lightly branded dorsally for orientation. Retinas were fixed in 4% PFA for 30 min and then permeabilized in PBS containing 0.5% Triton X-100 for 30 min. Primary antibodies used were as follows: Goat anti-S-opsin (Santa Cruz sc-14363, 1:1,000) and rabbit anti-M-opsin (Sigma AB5405, 1:1,000). Secondary antibodies used were as follows: donkey anti-goat Alexa 555 (Invitrogen A21432, 1:1,000) and donkey anti-rabbit Alexa 488 (Invitrogen A21206, 1:1,000). Additional details are described in *SI Appendix, SI Materials and Methods*.

Data, Materials, and Software Availability. RNA-seq data are available under GEO accession numbers GSE249756 (64) and GSE269667 (65). Analysis of differentially expressed genes in WT and *samd7*$^{-/-}$ zebrafish 5-dpf whole eyes, FAC-sorted *thrb:tdTomato*$^+$ cells, and adult retina is available in Datasets S1–S3, respectively. Analysis of differentially expressed genes in WT and *samd7*$^{minus10A/minus10A}$ mouse retina is in Dataset S4.

ACKNOWLEDGMENTS. We thank Dr. Rachel Wong (University of Washington) for providing the *Tg(thrb:Tomato)q22Tg* zebrafish line, Dr. Shoji Kawamura (University of Tokyo) for the *Tg(-5.5opn1sw1:EGFP)kj9Tg* and *Tg(-5opn1sw2:EGFP)kj11Tg* lines, Dr. Yoshitaka Fukada (University of Tokyo) for the *Tg(rho:EGFP)ja2Tg* line, Dr. David Hyde (University of Notre Dame) for the green opsin antibody, and Dr. Michael Nonet (Washington University in St. Louis) for Cas9 protein. We also thank the following centers at Washington University in St. Louis for their support: the Genome Technology Access Core (GTAC) in the Department of Genetics for library preparation and RNA-sequencing, the Flow Cytometry Core in the Department of Pathology and Immunology for FACS services, the Washington University Center for Cellular Imaging (WUCCI) for use of the LSM980 confocal microscope, the James Skeath lab for use of the LSM700 confocal microscope, Washington University's Zebrafish Facility for zebrafish care and maintenance, and the Genome Engineering and Stem Cell Center at Washington University (GESC) for the generation of *Samd7* mutant mice. This work was funded by the NIH: EY030075 (to J.C.C.), EY030912 (to V.J.K), and S10MH126964 (to WUCCI). We also acknowledge support to the Gavin Herbert Eye Institute at the University of California, Irvine, from an unrestricted grant from Research to Prevent Blindness and from NIH core grant P30 EY034070.

1. T. Baden, D. Osorio, The retinal basis of vertebrate color vision. *Annu. Rev. Vis. Sci.* **5**, 177–200 (2019).
2. S. P. Collin *et al.*, Ancient colour vision: Multiple opsin genes in the ancestral vertebrates. *Curr. Biol.* **13**, 864–865 (2003).
3. S. P. Collin, W. I. L. Davies, N. S. Hart, D. M. Hunt, The evolution of early vertebrate photoreceptors. *Philos. Trans. R. Soc. B Biol. Sci.* **364**, 2925–2940 (2009).
4. J. M. Angueyra *et al.*, Transcription factors underlying photoreceptor diversity. *Elife* **12**, e81579 (2023).
5. Y. Ogawa, J. C. Corbo, Partitioning of gene expression among zebrafish photoreceptor subtypes. *Sci. Rep.* **11**, 1–13 (2021).
6. A. Chinen, T. Hamaoka, Y. Yamada, S. Kawamura, Gene duplication and spectral diversification of cone visual pigments of zebrafish. *Genetics* **163**, 663–675 (2003).
7. W. I. L. Davies, S. P. Collin, D. M. Hunt, Molecular ecology and adaptation of visual photopigments in craniates. *Mol. Ecol.* **21**, 3121–3158 (2012).
8. A. P. Oel *et al.*, Nrl is dispensable for specification of rod photoreceptors in adult zebrafish despite its deeply conserved requirement earlier in ontogeny. *iScience* **23**, 101805 (2020).
9. F. Liu *et al.*, Rod genesis driven by mafba in an nrl knockout zebrafish model with altered photoreceptor composition and progressive retinal degeneration. *PLoS Genet.* **18**, 1–30 (2022).
10. S. Xie *et al.*, Knockout of Nr2e3 prevents rod photoreceptor differentiation and leads to selective L-/M-cone photoreceptor degeneration in zebrafish. *Biochim. Biophys. Acta Mol. Basis Dis.* **1865**, 1273–1283 (2019).
11. Y. Ogawa, T. Shiraki, Y. Fukada, D. Kojima, Foxq2 determines blue cone identity in zebrafish. *Sci. Adv.* **7**, 1–16 (2021).
12. K. Alvarez-Delfin *et al.*, Tbx2b is required for ultraviolet photoreceptor cell specification during zebrafish retinal development. *Proc. Natl. Acad. Sci. U.S.A.* **106**, 2023–2028 (2009).
13. S. C. Suzuki *et al.*, Cone photoreceptor types in zebrafish are generated by symmetric terminal divisions of dedicated precursors. *Proc. Natl. Acad. Sci. U.S.A.* **110**, 15109–15114 (2013).
14. L. I. Volkov *et al.*, Thyroid hormone receptors mediate two distinct mechanisms of long-wavelength vision. *Proc. Natl. Acad. Sci. U.S.A.* **117**, 15262–15269 (2020).
15. M. G. DuVal, A. P. Oel, W. T. Allison, Gdf6a is required for cone photoreceptor subtype differentiation and for the actions of tbx2b in determining rod versus cone photoreceptor fate. *PLoS One* **9**, e92991 (2014).
16. Y. Ogawa *et al.*, Six6 and Six7 coordinately regulate expression of middle-wavelength opsins in zebrafish. *Proc. Natl. Acad. Sci. U.S.A.* **116**, 4651–4660 (2019).
17. N. J. Nadolski, S. D. Balay, C. X. L. Wong, A. J. Waskiewicz, J. C. Hocking, Abnormal cone and rod photoreceptor morphogenesis in gdf6a mutant zebrafish. *Invest. Ophthalmol. Vis. Sci.* **61**, 9 (2020).
18. Y. Ogawa, T. Shiraki, D. Kojima, Y. Fukada, Homeobox transcription factor Six7 governs expression of green opsin genes in zebrafish. *Proc. R. Soc. B: Biol. Sci.* **282**, 1–8 (2015).
19. H. Nunley *et al.*, Defect patterns on the curved surface of fish retinae suggest a mechanism of cone mosaic formation. *PLoS Comput. Biol.* 16, e1008437 (2020).
20. C. Deveau *et al.*, Thyroid hormone receptor beta mutations alter photoreceptor development and function in Danio rerio (zebrafish). *PLoS Genet.* **16**, e10088 (2020).
21. H. Fujieda, R. Bremner, A. J. Mears, H. Sasaki, Retinoic acid receptor-related orphan receptor α regulates a subset of cone genes during mouse retinal development. *J. Neurochem.* **108**, 91–101 (2009).
22. L. Jia *et al.*, Retinoid-related orphan nuclear receptor RORβ is an early-acting factor in rod photoreceptor development. *Proc. Natl. Acad. Sci. U.S.A.* **106**, 17534–17539 (2009).
23. A. J. Mears *et al.*, Nrl is required for rod photoreceptor development. *Nat. Genet.* **29**, 447–452 (2001).
24. J. Chen, A. Rattner, J. Nathans, The rod photoreceptor-specific nuclear receptor Nr2e3 represses transcription of multiple cone-specific genes. *J. Neurosci.* **25**, 118–129 (2005).
25. J. C. Corbo, C. L. Cepko, A hybrid photoreceptor expressing both rod and cone genes in a mouse model of enhanced S-cone syndrome. *PLoS Genet.* **1**, e11 (2005).
26. P. Mattar *et al.*, A Casz1–NuRD complex regulates temporal identity transitions in neural progenitors. *Sci. Rep.* **11**, 1–12 (2021).
27. A. Onishi *et al.*, The orphan nuclear hormone receptor ERRβ controls rod photoreceptor survival. *Proc. Natl. Acad. Sci. U.S.A.* **107**, 11579–11584 (2010).
28. L. Ng *et al.*, A thyroid hormone receptor that is required for the development of green cone photoreceptors. *Nat. Genet.* **27**, 94–98 (2001).
29. M. R. Roberts, A. Hendrickson, C. R. McGuire, T. A. Reh, Retinoid X receptor is necessary to establish the S-opsin gradient in cone photoreceptors of the developing mouse retina. *Invest. Ophthalmol. Vis. Sci.* **46**, 2897–2904 (2005)
30. H. Liu *et al.*, NeuroD1 regulates expression of thyroid hormone receptor 2 and cone opsins in the developing mouse retina. *J. Neurosci.* **28**, 749–756 (2008).
31. A. Onishi *et al.*, Pias3-dependent SUMOylation directs rod photoreceptor development. *Neuron* **61**, 234–246 (2009).
32. C. K. Campla *et al.*, Pias3 is necessary for dorso-ventral patterning and visual response of retinal cones but is not required for rod photoreceptor differentiation. *Biol. Open* **6**, 881–890 (2017).
33. J. de Melo, G. H. Peng, S. Chen, S. Blackshaw, The spalt family transcription factor Sall3 regulates the development of cone photoreceptors and retinal horizontal interneurons. *Development* **138**, 2325–2336 (2011).
34. S. Satoh *et al.*, The spatial patterning of mouse cone opsin expression is regulated by bone morphogenetic protein signaling through downstream effector COUP-TF nuclear receptors. *J. Neurosci.* **29**, 12401–12411 (2009).
35. O. B. Sawant *et al.*, The circadian clock gene Bmal1 controls thyroid hormone-mediated spectral identity and cone photoreceptor function. *Cell Rep.* **21**, 692–706 (2017).
36. F. M. Nadal-Nicolás *et al.*, True S-cones are concentrated in the ventral mouse retina and wired for color detection in the upper visual field. *Elife* **9**, 1–30 (2020).
37. S. Haverkamp, The primordial, blue-cone color system of the mouse retina. *J. Neurosci.* **25**, 5438–5445 (2005).
38. Y. Omori *et al.*, Samd7 is a cell type-specific PRC1 component essential for establishing retinal rod photoreceptor identity. *Proc. Natl. Acad. Sci. U.S.A.* **114**, E8264–E8273 (2017).
39. T. P. Wilm, L. Solnica-Krezel, Essential roles of a zebrafish prdm1/blimp1 homolog in embryo patterning and organogenesis. *Development* **132**, 393–404 (2005).
40. J. A. Brzezinski IV, D. A. Lamba, T. A. Reh, Blimp1 controls photoreceptor versus bipolar cell fate choice during retinal development. *Development* **137**, 619–629 (2010).
41. M. Takechi, S. Kawamura, Temporal and spatial changes in the expression pattern of multiple red and green subtype opsin genes during zebrafish development. *J. Exp. Biol.* **208**, 1337–1345 (2005).
42. E. Cau, B. Ronsin, L. Bessière, P. Blader, A. Notch-mediated, temporal asymmetry in BMP pathway activation promotes photoreceptor subtype diversification. *PLoS Biol.* **17**, 1–22 (2019).
43. J. M. Fadool, Development of a rod photoreceptor mosaic revealed in transgenic zebrafish. *Dev. Biol.* **258**, 277–290 (2003).
44. R. D. Mackin *et al.*, Endocrine regulation of multichromatic color vision. *Proc. Natl. Acad. Sci. U.S.A.* **116**, 16882–16891 (2019).
45. M. Takechi, S. Seno, S. Kawamura, Identification of cis-acting elements repressing blue opsin expression in zebrafish UV cones and pineal cells. *J. Biol. Chem.* **283**, 31625–31632 (2008).
46. C. Guo *et al.*, Intrinsic expression of a multiexon type 3 deiodinase gene controls zebrafish embryo size. *Endocrinology (United States)* **155**, 4069–4080 (2014).
47. A. A. Farre *et al.*, Long wavelength-sensing cones of zebrafish retina exhibit multiple layers of transcriptional heterogeneity. *Front. Cell Neurosci.* **17**, 1–23 (2023).
48. Z. Jiang *et al.*, Exdpf is a key regulator of exocrine pancreas development controlled by retinoic acid and ptf1a in zebrafish. *PLoS Biol.* **6**, 2450–2464 (2008).

49. W. T. Allison *et al.*, Ontogeny of cone photoreceptor mosaics in zebrafish. *J. Comp. Neurol.* **518**, 4182–4195 (2010).
50. J. Wan, D. Goldman, Retina regeneration in zebrafish. *Curr. Opin. Genet. Dev.* **40**, 41–47 (2016).
51. R. Ramachandran, X. F. Zhao, D. Goldman, Insm1a-mediated gene repression is essential for the formation and differentiation of Müller glia-derived progenitors in the injured retina. *Nat. Cell Biol.* **14**, 1013–1023 (2012).
52. R. Ramachandran, B. V. Fausett, D. Goldman, Ascl1a regulates Müller glia dedifferentiation and retinal regeneration through a Lin-28-dependent, let-7 microRNA signalling pathway. *Nat. Cell Biol.* **12**, 1101–1107 (2010).
53. K. D. Larison, R. Bremiller, Early onset of phenotype and cell patterning in the embryonic zebrafish retina. *Development* **109**, 567–576 (1990).
54. S. L. Renninger, M. Gesemann, S. C. Neuhauss, Cone arrestin confers cone vision of high temporal resolution in zebrafish larvae. *Eur. J. Neurosci.* **33**, 658–667 (2011).
55. M. Aramaki *et al.*, Transcriptional control of cone photoreceptor diversity by a thyroid hormone receptor. *Proc. Natl. Acad. Sci. U.S.A.* **119**, 2017 (2022).
56. M. B. Toomey *et al.*, A mechanism for red coloration in vertebrates. *Curr. Biol.* **32**, 4201–4214.e12 (2022).
57. M. Yamagata, W. Yan, J. R. Sanes, A cell atlas of the chick retina based on single-cell transcriptomics. *Elife* **10**, 1–39 (2021).
58. E. D. Thomas *et al.*, Cell-specific cis-regulatory elements and mechanisms of non-coding genetic disease in human retina and retinal organoids. *Dev. Cell* **57**, 820–836.e6 (2022).
59. M. Bauwens *et al.*, Mutations in SAMD7 cause autosomal-recessive macular dystrophy with or without cone dysfunction. *Am. J. Hum. Genet.* **111**, 393–402 (2024).
60. H. M. T. Choi *et al.*, Third-generation in situ hybridization chain reaction: Multiplexed, quantitative, sensitive, versatile, robust. *Development* **145**, dev165753 (2018).
61. T. S. Vihtelic, C. J. Doro, D. R. Hyde, Cloning and characterization of six zebrafish photoreceptor opsin cDNAs and immunolocalization of their corresponding proteins. *Vis. Neurosci.* **16**, 571–585 (1999).
62. K. E. Ile *et al.*, Zebrafish class 1 phosphatidylinositol transfer proteins: PITPβ and double cone cell outer segment integrity in retina. *Traffic* **11**, 1151–1167 (2010).
63. J. Schindelin *et al.*, Fiji: An open-source platform for biological-image analysis. *Nat. Methods* **9**, 676–682 (2012).
64. L. I. Volkov, Y. Ogawa, J. C. Corbo, Samd7 preserves cell identity and enforces the 'one neuron-one receptor' rule in vertebrate photoreceptors. Gene Expression Omnibus. https://www.ncbi.nlm.nih.gov/geo/query/acc.cgi?acc=GSE249756. Deposited 8 December 2023.
65. L. I. Volkov, R. Somjee, J. C. Corbo, Samd7 preserves cell identity and enforces the 'one neuron-one receptor' rule in vertebrate photoreceptors. Gene Expression Omnibus. https://www.ncbi.nlm.nih.gov/geo/query/acc.cgi?acc=GSE269667. Deposited 12 June 2024.